Journal of Magnetic Resonance **147,** 238–249 (2000)
doi:10.1006/jmre.2000.2174, available online at http://www.idealibrary.com on IDEAL®

Multiple-Quantum Cross-Polarization and Two-Dimensional MQMAS NMR of Quadrupolar Nuclei

Sharon E. Ashbrook*,† and Stephen Wimperis*

*School of Chemistry, University of Exeter, Stocker Road, Exeter EX4 4QD; and †Physical Chemistry Laboratory, University of Oxford, South Parks Road, Oxford OX1 3QZ, United Kingdom

Received April 13, 2000; revised July 18, 2000

Cross-polarization from ^{1}H to the multiple-quantum coherences of a quadrupolar nucleus is used in combination with the two-dimensional multiple-quantum magic angle spinning (MQMAS) NMR experiment in order to extract high-resolution CPMAS NMR spectra. The technique is demonstrated on ^{23}Na ($S = \frac{3}{2}$), ^{17}O, ^{27}Al (both $S = \frac{5}{2}$), and ^{45}Sc ($S = \frac{7}{2}$) nuclei, showing the applicability of multiple-quantum cross-polarization to systems with differing spin quantum number, gyromagnetic ratio, and relative nuclide abundance. The utility of this two-dimensional MAS NMR experiment for spectral editing and site-specific measurement of cross-polarization intensities is demonstrated. The possibility of direct cross-polarization to higher order multiple-quantum coherences is also considered and three-, five-, and seven-quantum cross-polarized ^{45}Sc MAS NMR spectra are presented. © 2000 Academic Press

1. INTRODUCTION

The use of cross-polarization to enhance NMR signals of nuclei with low gyromagnetic ratios is routine in the study of spin $I = S = \frac{1}{2}$ systems, such as ^{1}H/^{13}C, in solids, particularly when combined with magic angle spinning (MAS) (*1*, *2*). The ability of this technique to "edit" NMR spectra on the basis of the spatial proximity of nuclei has also proven to be a valuable tool in structure determination. In comparison, the dynamics of cross-polarization to or from quadrupolar nuclei are inherently more complex, particularly under MAS conditions, and signal enhancements are observed only rarely. The use of cross-polarization in a spectral editing capacity still holds great potential for the investigation of spatial relationships, however, and studies of cross-polarization from $I = \frac{1}{2}$ nuclei to half-integer quadrupolar nuclei such as ^{11}B, ^{23}Na (both $S = \frac{3}{2}$), ^{17}O, ^{27}Al, ^{95}Mo (all $S = \frac{5}{2}$), and ^{43}Ca ($S = \frac{7}{2}$) have been performed (*3–12*).

Detailed structural information is often difficult to extract from NMR spectra of quadrupolar nuclei in solids owing to the presence of inhomogeneous second-order quadrupolar broadening. This broadening cannot be fully removed by MAS alone and hinders the resolution of chemically and crystallographically distinct sites (*13*). The two-dimensional multiple-quantum MAS (MQMAS) experiment, first proposed by Frydman and colleagues in 1995 (*14, 15*), refocuses the second-order broadening and allows high-resolution NMR spectra of half-integer quadrupolar nuclei to be obtained using only conventional MAS hardware. The method has aroused great interest since its introduction, a number of promising variants have been proposed, and many applications to systems such as minerals, glasses, zeolites, and other amorphous solids have been demonstrated (*16–18*).

It has been shown by Pruski *et al.* and Fernandez *et al.* that it is possible to introduce a cross-polarization step into the MQMAS experiment, allowing editing of high-resolution spectra of quadrupolar nuclei based upon the distance from an abundant spin $I = \frac{1}{2}$ nucleus, such as ^{1}H or ^{19}F (*19*, *20*). Such an experiment, combining these two important techniques, offers the prospect of obtaining structural information from a wide range of inorganic solids. The experiment proposed by Pruski *et al.* involves an initial conventional cross-polarization step, transferring magnetization from the spin $I = \frac{1}{2}$ nucleus to the quadrupolar nucleus during a period of simultaneous spin locking. The single-quantum coherences created in this step are then converted into a population difference across the quadrupolar $m_S = \pm\frac{1}{2}$ eigenstates by a selective 90° pulse. Subsequently, multiple-quantum coherences are excited by a single, full-power radiofrequency pulse and an MQMAS experiment, in this particular case the *z*-filter experiment of Amoureux *et al.* (*21*), is performed.

Recently, an alternative method for the combination of cross-polarization and MQMAS has been proposed by Ashbrook *et al.* (*22*). In this technique, the polarization of the spin $I = \frac{1}{2}$ nucleus is transferred directly to the multiple-quantum coherences of a quadrupolar nucleus during the spin-locking period. These multiple-quantum coherences are then correlated with single-quantum coherences in a two-dimensional MQMAS experiment. This approach also allows editing of the high-resolution NMR spectrum and appears to be the most simple and efficient way of combining the two techniques. Multiple-quantum cross-polarization to half-integer quadrupolar nuclei has also been observed by Lim and Grey (*23, 24*) and Rovnyak *et al.* (*25*).

The purpose of the present work is to demonstrate the utility

1090-7807/00 $35.00

of this combination of multiple-quantum cross-polarization (MQCP) and the MQMAS experiment on a variety of samples and on quadrupolar nuclei with spin quantum number $S = \frac{3}{2}$ (^{23}Na), $S = \frac{5}{2}$ (^{17}O and ^{27}Al), and $S = \frac{7}{2}$ (^{45}Sc). Examples of cross-polarization to higher order multiple-quantum coherences are also presented and the uses and possible limitations of this method are discussed.

2. BACKGROUND TO MULTIPLE-QUANTUM CROSS-POLARIZATION

Cross-polarization between spin $I = \frac{1}{2}$ and $S = \frac{1}{2}$ systems is a relatively simple process. For a static sample, it can be shown that there is a unique "Hartmann–Hahn matching condition" (*1*), where polarization is transferred between the two sets of nuclei, given by

$$\omega_{1I} = \omega_{1S}, \qquad [1]$$

where $\omega_{1I} = -\gamma_I B_{1I}$ and $\omega_{1S} = -\gamma_S B_{1S}$ are the inherent nutation rates (or, in common parlance, the "radiofrequency field strengths") produced by the radiofrequency fields B_{1I} and B_{1S} applied to the I and S nuclei, respectively. The rotation of the sample that occurs during MAS introduces a time dependence into the dipolar interaction between the I and S spins and, consequently, optimum polarization transfer is not obtained at the condition in Eq. [1], but at the modified Hartmann–Hahn condition (*26*),

$$\omega_{1I} = \omega_{1S} \pm n\omega_R, \qquad [2]$$

where ω_R is the spinning frequency and n is an integer, usually 1 or 2.

If S is a quadrupolar nucleus ($S \geq 1$) then the matching conditions for cross-polarization are not as simple as those described above for $I = S = \frac{1}{2}$ (*27–32*). A nucleus with spin quantum number S has $2S + 1$ energy levels and, therefore, $S(2S + 1)$ transition frequencies. In the eigenbasis of the on-resonance spin-locking Hamiltonians of the I and S spins, however, only $(S + \frac{1}{2})^2$ transitions (if S is half-integral) will have matrix elements in the IS dipolar coupling Hamiltonian linking them to the I spin. Thus, only these $(S + \frac{1}{2})^2$ transitions are available for cross-polarization (*31, 32*). In the spin-locking eigenbasis, the frequencies of these transitions (the actual nutation rates) depend, in general, on both the radiofrequency field strength ω_{1S} and the quadrupolar splitting parameter, ω_Q, where

$$\omega_Q = \frac{\omega_Q^{PAS}}{2}(3\cos^2\theta - 1 + \eta\sin^2\theta\cos 2\phi) \qquad [3a]$$

$$\omega_Q^{PAS} = \frac{3e^2qQ}{4S(2S-1)\hbar}. \qquad [3b]$$

The angles θ and ϕ describe the orientation of the principal axis system (PAS) of the quadrupole tensor in the laboratory frame (these will become time dependent if the sample is rotated, for example, as during MAS) and all other symbols have their usual meanings.

In a static sample, therefore, cross-polarization occurs when the I-spin nutation rate ω_{1I} is matched to any one of the $(S + \frac{1}{2})^2$ allowed nutation rates of the half-integer quadrupolar spin S (*31, 32*). This matching condition can be written

$$\omega_{1I} = \omega_{r,s}, \qquad [4]$$

where $\omega_{r,s}$ is one of the permitted S-spin nutation rates and r and s are shorthand labels for $|r\rangle$ and $|s\rangle$, two of the $2S + 1$ eigenstates of the spin-locking Hamiltonian of spin S. Only the transition $|r\rangle \leftrightarrow |s\rangle$ is polarized at this particular matching condition. However, it is important to note that this transition cannot, in general, be classified as (say) either a single-quantum or a three-quantum coherence as it is a transition in the spin-locking eigenbasis and not in the normal rotating frame (*32*). At the end of the spin-locking period, when it is useful to view the system in the rotating frame again, it has been shown that this spin-locking transition $|r\rangle \leftrightarrow |s\rangle$ is "mixed" by the coordinate transformation into all possible S-spin populations and coherence orders (i.e., single-, two-, and three-quantum coherences and, if $S > \frac{3}{2}$, higher order multiple-quantum coherences as well) (*32*). Thus, in general, single- and multiple-quantum cross-polarization are not distinct processes: they share the same matching conditions (but not necessarily the same *optimum* matching conditions) and always occur together (*32*).

In the past, cross-polarization to a quadrupolar nucleus has usually been discussed using the theoretical simplification that $\omega_Q \gg \omega_{1S}$ (*31, 33*). In this special limiting case, the on-resonance spin-locking eigenbasis of the S spin has a much closer relationship with the normal rotating frame and now only $S + \frac{1}{2}$ transitions (if S is half-integral) are linked to the I spin by the IS dipolar coupling Hamiltonian and are, therefore, available for cross-polarization. In this limit only, therefore, single- and three-quantum cross-polarization are distinct processes and will occur at the following matching conditions:

$$\omega_{1I} = \omega_{r,s} = (S + \tfrac{1}{2})\omega_{1S} \qquad [5a]$$

$$\omega_{1I} = \omega_{r',s'} = \frac{k\omega_{1S}^3}{\omega_Q^2}, \qquad [5b]$$

respectively (*31, 32*). The well-known expressions given in Eqs. [5a] and [5b] are just special cases of a general matching condition for on-resonance n-quantum cross-polarization in the limit $\omega_Q \gg \omega_{1S}$, given by

$$\omega_{1I} = \omega_{r,s} = \frac{k\omega_{1S}^{n}}{\omega_{Q}^{n-1}} \quad [6a]$$

$$k = \frac{2^{(1-n)}}{(n-1)!^{2}} \frac{(S + n/2)!}{(S - n/2)!}, \quad [6b]$$

where $n = 1, 3, 5, 7, 9, \ldots$, etc.

It has been argued that cross-polarization to the central transition (single-quantum) of a half-integer quadrupolar nucleus may be easily observed by matching ω_{1I} to the $\omega_{r,s} = (S + \frac{1}{2})\,\omega_{1S}$ nutation rate as in Eq. [5a], but that the very low multiple-quantum nutation rates in Eqs. [5b] and [6] mean that cross-polarization directly to multiple-quantum coherence is much more difficult (*33*). However, even for systems where $\omega_{Q}^{PAS} \gg \omega_{1S}$, in a static powder many crystallites will still have $\omega_{Q} \lesssim \omega_{1S}$, while in a powder undergoing MAS all crystallites will have $\omega_{Q} \lesssim \omega_{1S}$ during part of the rotor cycle. Although felicitous from a theoretical point of view, therefore, the limiting case $\omega_{Q} \gg \omega_{1S}$ does not appear to correspond closely to experimental reality, even if a low ω_{1S} field strength is used. Instead, it is the general case, described above, where $\omega_{Q} \sim \omega_{1S}$ and where single- and multiple-quantum cross-polarization are not distinct processes, that seems more appropriate. It has been shown in Ref. (*32*) that, when $\omega_{Q} \sim \omega_{1S}$, some of the $(S + \frac{1}{2})^{2}$ spin-locking transitions still mix strongly into multiple-quantum coherences and a few have nutation rates $\omega_{r,s}$ that are greater than ω_{1S}, in some cases, several times greater. As a result, offset effects will be relatively unimportant and there will be no great difficulty in matching ω_{1I} to these nutation rates, as has been recently demonstrated for three- and five-quantum cross-polarization in static samples (*32*).

The use of MAS leads to further complications in a quadrupolar spin system. Not only does the IS dipolar interaction become time dependent, but a time dependence is also introduced into the quadrupolar interaction and, therefore, into the S-spin nutation rates, $\omega_{r,s}$, as well. For static samples, it has been recently been shown that single- and multiple-quantum quadrupolar nutation spectra can be used to measure the same $(S + \frac{1}{2})^{2}$ nutation frequencies as those available for matching in a single- or multiple-quantum cross-polarization experiment (*32*). Therefore, nutation spectra can be used to determine independently the optimum matching conditions for single- and multiple-quantum cross-polarization (*32*). Under MAS conditions, it is still possible to record single- and multiple-quantum quadrupolar nutation spectra and, particularly when the spinning speed is small, these do not differ greatly from static nutation spectra (*34, 35*). As the MAS rate is increased, however, nutation spectra break up into spinning sidebands (*34, 35*) and it might therefore be expected that the matching conditions observed in single- and multiple-quantum cross-polarization will show sidebands that are dependent upon the spinning speed.

The efficiency of cross-polarization to a quadrupolar nucleus under MAS conditions also depends upon the extent to which spin locking can be maintained in the presence of the time-dependent quadrupolar interaction. An adiabatic-passage parameter has been introduced by Vega (*36*), which, using our definition of ω_{Q}^{PAS}, is given by

$$\alpha = \frac{\omega_{1S}^{2}}{2\omega_{Q}^{PAS}\omega_{R}}. \quad [7]$$

If $\alpha \gg 1$ then the rotor-driven modulation of the spin-locking eigenstates occurs adiabatically, while the modulation is sudden if $\alpha \ll 1$. In both extremes spin locking is possible. If the experiment is performed in the intermediate regime where $\alpha \sim 1$, however, then spin locking is not maintained and the cross-polarization efficiency decreases correspondingly (*36*). Although the matching conditions for cross-polarization are predicted and observed to be approximately the same for static and spinning samples, the intensity of the CPMAS signal may be significantly affected by the efficiency with which the S-spin transitions are spin-locked. This observation applies equally to single- and multiple-quantum cross-polarization since, as noted above, in general the two processes originate from the same S-spin transitions in the spin-locking eigenbasis.

A full discussion of the theoretical basis of cross-polarization directly to the multiple-quantum coherences of a quadrupolar nucleus under MAS conditions will be presented elsewhere.

3. EXPERIMENTAL RESULTS

Experiments were performed on a Bruker MSL 400 spectrometer operating at 400.1, 105.8, 104.3, 54.2, and 97.2 MHz for ^{1}H, ^{23}Na, ^{27}Al, ^{17}O, and ^{45}Sc, respectively. Powdered samples were packed into 4-mm MAS rotors. All radiofrequency field strengths were calibrated independently on a variety of samples and so quoted values are approximate only. Owing to the many theoretical factors affecting the optimium matching conditions for multiple-quantum cross-polarization, all cross-polarization steps in this work were carried out at matching conditions that were found experimentally by a combination of direct searching and nutation spectroscopy (*32*).

3.1. Two-Dimensional Multiple-Quantum Cross-Polarization and MQMAS

Two-dimensional multiple-quantum cross-polarized MQMAS experiments were performed using the pulse sequences and coherence transfer pathways (*37*) shown in Fig. 1. In all versions of the experiments ^{1}H magnetization is transferred directly to the multiple-quantum coherences of the quadrupolar S nucleus during the spin-locking period or "contact time." All three pulse sequences are used in this paper for three-quantum cross-polarization (solid pathways), while some five- and seven-quantum cross-polarization experiments are also performed

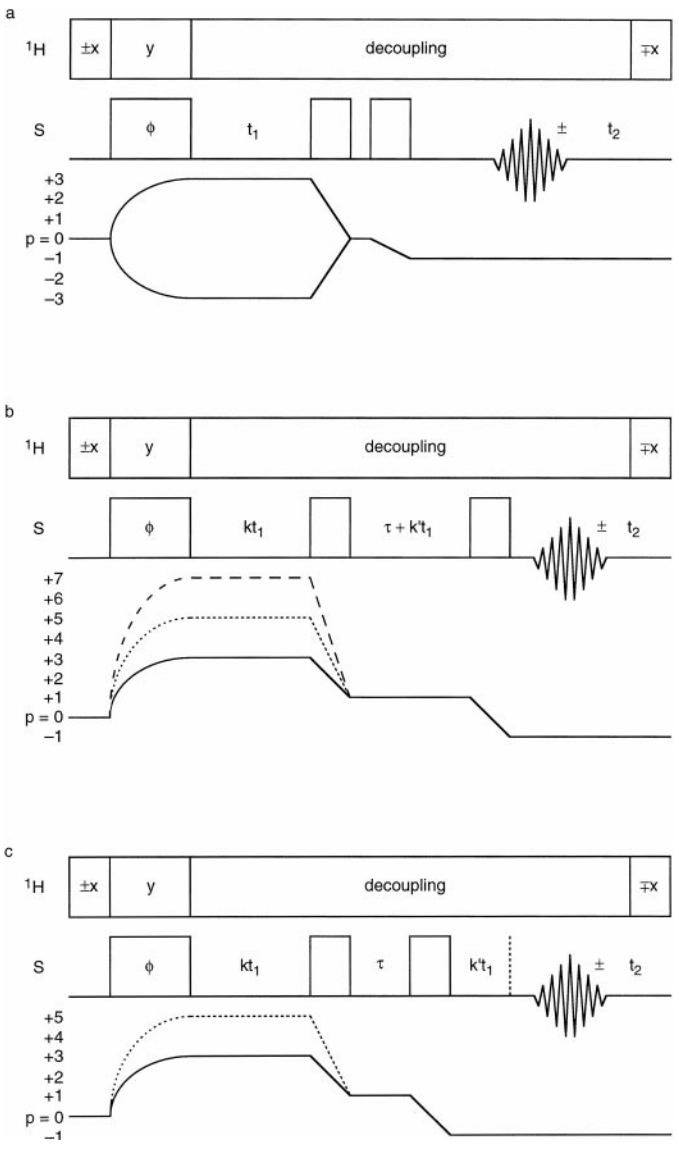

FIG. 1. Pulse sequences and coherence transfer pathway diagrams for (a) three-quantum cross-polarized *z*-filtered MAS NMR experiment and (b) and (c) multiple-quantum cross-polarized phase-modulated split-t_1 MAS experiments. The split-t_1 coefficients k and k' are functions of both the multiple-quantum coherence order p and the spin quantum number S. In all experiments the multiple-quantum coherence is excited directly by the cross-polarization process, with three-, five-, and seven-quantum cross-polarized experiments denoted by solid, dotted, and dashed coherence pathways, respectively. All three experiments make use of a "flip-back" pulse to aid the recovery of the ^{1}H magnetization.

(dotted and dashed coherence transfer pathways, respectively). In order to cancel multiple-quantum coherences arising from the equilibrium magnetization of the S spin, the initial ^{1}H pulse is phase alternated in concert with the receiver: the effectiveness of this procedure has been verified (*22*). All experiments in Fig. 1 also make use of a "flip-back" pulse to aid the recovery of the ^{1}H equilibrium magnetization, while ^{1}H decoupling is performed throughout. Phase cycles for all of the MQCP-MQMAS experiments used in this paper are easily derived from Fig. 1 (*37*) or are available from the authors on request.

In the amplitude-modulated MQMAS experiment in Fig. 1a, phase cycling is used to select both $p = \pm n$ coherences during t_1. In order to ensure absorptive two-dimensional lineshapes, a *z*-filter (*21, 38*) is included in the sequence, i.e., a pulse is used to convert the multiple-quantum coherences to populations while another pulse reads these out as observable single-quantum coherences.

In contrast, in the pulse sequences shown in Figs. 1b and 1c, phase cycling ensures that only $p = +n$ coherences are selected after the spin-locking period. These coherences are then correlated with single-quantum coherences in a phase-modulated split-t_1 MQMAS experiment (*39–42*). Absorptive two-dimensional lineshapes are obtained by recording the whole echo during acquisition. In split-t_1 experiments, the t_1 period is split between multiple- and single-quantum evolution in order to refocus the inhomogeneous quadrupolar broadening at the end of t_1. As a result, the ridge lineshapes in the two-dimensional spectrum appear parallel to the F_2 axis, without the need for a shearing transformation, and the high-resolution isotropic projection is directly available. The exact position of the single-quantum t_1 evolution period in these experiments, i.e., either before (Fig. 1b) or after (Fig. 1c) the final pulse, is determined by the sign of the MQMAS ratio for the particular spin and coherence order (*40*). If the MQMAS ratio is negative, e.g., $-7/9$ for $S = \frac{3}{2}$ three-quantum, the second part of the t_1 period is placed before the final pulse, as in Fig. 1b. Alternatively, if the MQMAS ratio is positive, e.g., 19/12 for $S = \frac{5}{2}$ three-quantum, then the single-quantum t_1 period occurs after the final pulse, as in Fig. 1c. The values of k and k' are also determined by the MQMAS ratio for the particular spin system and coherence order. For example, the MQMAS ratio is $-7/9$ for $S = \frac{3}{2}$ and, therefore, $k = 9/16$ and $k' = 7/16$.

Figure 2a shows the conventional ^{23}Na ($S = \frac{3}{2}$) MAS NMR spectrum of sodium citrate dihydrate ($Na_3C_6H_5O_7.2H_2O$) recorded with ^{1}H decoupling. The complex central-transition lineshape clearly reveals the presence of more than one distinct Na site. Figure 2b shows the corresponding ^{23}Na MAS NMR spectrum recorded with a single-quantum cross-polarization sequence involving transfer of magnetization from ^{1}H to ^{23}Na. Although this spectrum indicates that ^{1}H and ^{23}Na are sufficiently close in space for cross-polarization to occur, little indication of the number or nature of ^{23}Na nuclei involved is obtained. As expected, cross-polarization is inefficient in this system, achieving only 3% of the intensity of a conventional spectrum recorded with the same number of transients. It should also be noted that I to S cross-polarization depends upon the relaxation rate of the I spins, while conventional S-spin NMR depends upon the relaxation rate of the S spins (*2*). In systems such as ^{1}H/^{13}C this often means that a cross-polarization experiment can proceed with a shorter "recycle"

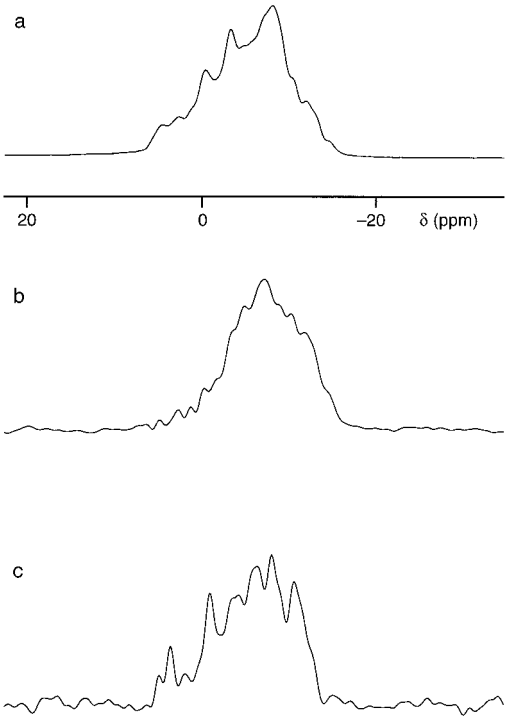

FIG. 2. (a) Conventional, (b) single-quantum cross-polarized, and (c) three-quantum cross-polarized ^{23}Na (105.8 MHz) MAS NMR spectra of sodium citrate dihydrate ($Na_3C_6H_5O_7.2H_2O$). In (a) 24 transients were averaged with a 2-s recycle interval, in (b) 48 transients were averaged with a 40-s recycle interval, and in (c) 192 transients were averaged with a 40-s recycle interval. Cross-polarization was performed with ^{23}Na radiofrequency field strengths of $\omega_{1S}/2\pi = 100$ kHz and with ^{1}H radiofrequency field strengths of $\omega_{1I}/2\pi$ of (b) 77 and (c) 35 kHz and with a contact time in both (b) and (c) of 1 ms. In all spectra the displayed spectral width is 6 kHz and the spinning rate was 6.5 kHz. The ppm scale is referenced to 1 M NaCl (aq).

interval than a conventional experiment, allowing an increase in the signal-to-noise obtained per unit time. However, in sodium citrate, where the relaxation of ^{23}Na appears to be much more efficient than that of ^{1}H, the conventional spectrum in Fig. 2a was able to be recorded with a recycle interval that was only 5% of the duration of that used for the cross-polarized spectrum in Fig. 2b. Fortunately for the prospects of single- and multiple-quantum cross-polarization, such an extreme difference between the I and S relaxation rates is untypical.

The three-quantum cross-polarized ^{23}Na MAS NMR spectrum shown in Fig. 2c was recorded with a cross-polarization sequence where ^{1}H magnetization is transferred directly to the three-quantum coherences of the ^{23}Na nucleus (*22, 32*). Again, a large loss in signal intensity is observed, with a three-quantum cross-polarized spectrum having only 1% of the intensity of a conventional spectrum recorded with the same number of transients. Moreover, the recycle interval used in the three-quantum cross-polarized spectrum in Fig. 2c is again a factor of 20 greater than that used in Fig. 2a. It should be noted, however, that the spectrum in Fig. 2c contains 6% of the intensity of a conventional three-quantum filtered spectrum (not shown) recorded with an equal number of transients.

The two-dimensional three-quantum ^{23}Na MAS NMR spectrum in Fig. 3a, recorded using a phase-modulated three-quantum split-t_1 pulse sequence (*39, 40*), shows clearly the presence of three ridge lineshapes parallel to the F_2 axis, corresponding to three distinct Na sites. The isotropic projection onto the F_1 axis reveals three peaks with approximately equal intensities. From the F_1 and F_2 positions of the centers of gravity of the ridge lineshapes, values of the isotropic chemical shift, δ_{CS}, and the quadrupolar product, $P_Q = (e^2qQ/h)(1 + \eta^2/3)^{1/2}$ (*43*), may be obtained. The values determined by this method (−2.0, 0.6, and 6.7 ppm and 1.65, 1.87, and 1.90 MHz for the peaks with F_1 shifts of 3, 11, and 25 ppm, respectively) agree with those found in the literature (*44*).

The two-dimensional three-quantum cross-polarized ^{23}Na MAS NMR spectrum displayed in Fig. 3b was recorded with the pulse sequence in Fig. 1b (solid pathway) with $k = 9/16$ and $k' = 7/16$. This spectrum clearly shows that cross-

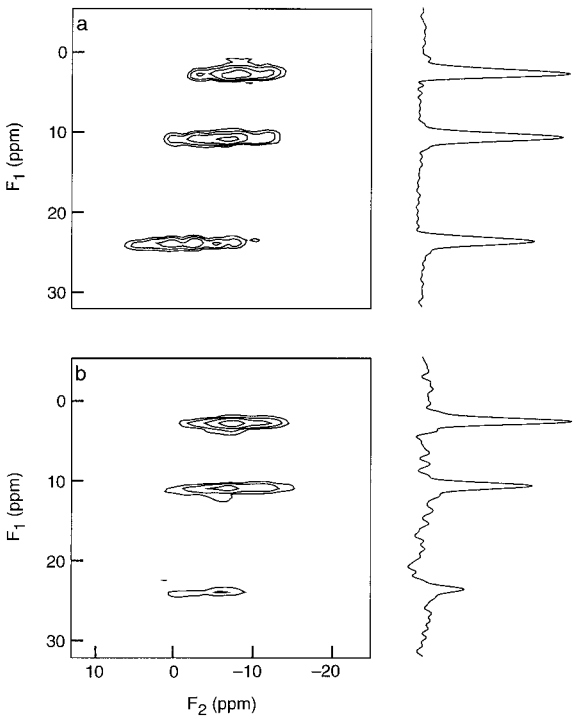

FIG. 3. Two-dimensional (a) three-quantum ^{23}Na MAS and (b) three-quantum cross-polarized ^{23}Na MAS NMR spectra of sodium citrate, recorded with (a) a conventional split-t_1 three-quantum experiment and (b) the pulse sequence shown in Fig. 1b with the solid coherence transfer pathway ($k = 9/16$, $k' = 7/16$). In (a) 96 transients were averaged for each of 192 t_1 increments of 50 μs with a recycle interval of 2 s and in (b) 192 transients were averaged for each of 192 t_1 increments of 50 μs with a recycle interval of 20 s. In both cases displayed F_1 and F_2 spectral widths are 4 kHz and the MAS rate was 6.5 kHz. Contour levels are shown at 8, 16, 32, and 64% of the maximum value. In (b) cross-polarization was performed with a ^{23}Na radiofrequency field strength of $\omega_{1S}/2\pi = 100$ kHz, a ^{1}H radiofrequency field strength of $\omega_{1I}/2\pi = 35$ kHz, and a contact time of 1 ms.

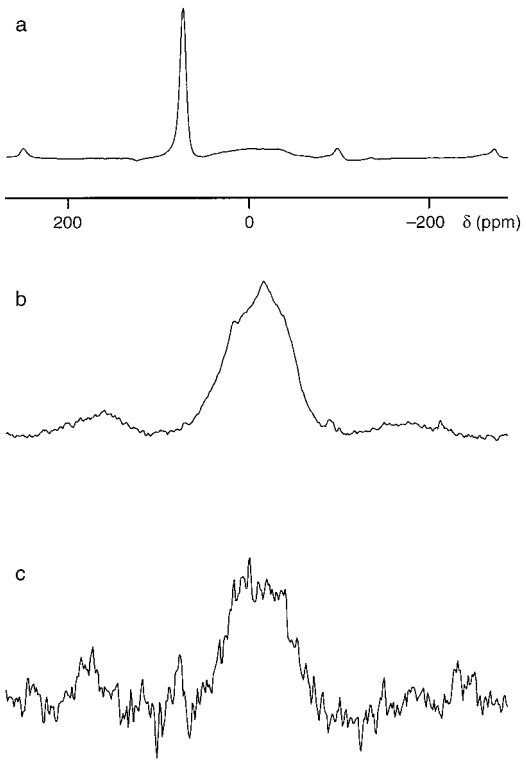

FIG. 4. (a) Conventional, (b) single-quantum cross-polarized, and (c) three-quantum cross-polarized ^{17}O (54.2 MHz) MAS NMR spectra of 35% isotopically enriched boehmite (AlO(OH)). In all experiments 1200 transients were averaged with a 1-s recycle interval. Cross-polarization was performed with ^{17}O radiofrequency field strengths of (b) $\omega_{1S}/2\pi$ = 25 kHz and (c) $\omega_{1S}/2\pi$ = 80 kHz, ^{1}H field strengths of (b) $\omega_{1I}/2\pi$ = 77 kHz and (c) $\omega_{1I}/2\pi$ = 50 kHz, and a contact time in both (b) and (c) of 100 μs. In all spectra the displayed spectral width is 30 kHz and the spinning rate was 9 kHz. The ppm scale is referenced to H_2O.

polarization to all three distinct Na sites is possible, a conclusion unobtainable from the cross-polarized spectra in Figs. 2b and 2c. The isotropic projection contains three ^{23}Na resonances, although it appears that cross-polarization to the ^{23}Na spins at $\delta \approx 25$ ppm in F_1 is less efficient, a result that might indicate a greater distance from ^{1}H. It should be noted, however, that other factors, such as the duration of the spin-locking period or the radiofrequency field strengths at which the experiment is performed, can affect cross-polarization intensities, particularly for quadrupolar nuclei.

3.2. Applications of Multiple-Quantum Cross-Polarized MQMAS Experiments

Cross-polarization proceeds via the dipolar coupling between spins I and S. In principle, therefore, this allows observation of only those S nuclei that are sufficiently close to an I spin for the pair to possess a significant dipolar coupling, i.e., the method can be used for spectral editing. Figure 4a shows the conventional ^{17}O ($S = \frac{5}{2}$) MAS NMR spectrum of 35% isotopically enriched boehmite (AlO(OH)) consisting of a sharp peak at 75 ppm and a broader resonance at −5 ppm. The ^{17}O MAS NMR spectrum in Fig. 4b was recorded using a conventional cross-polarization sequence and shows a single dominant resonance, corresponding to the broader peak discussed above. From the structure of boehmite it can be postulated that the sharper resonance, not observed in the cross-polarization spectrum, arises from ^{17}O nuclei in Al–O–Al linkages, whereas that at lower ppm corresponds to ^{17}O nuclei with directly bonded ^{1}H, i.e., Al–O–H linkages (*7*, *8*). The cross-polarization experiment has, therefore, edited the spectrum to enable selective observation of the Al–O–H oxygens. It is also significant that cross-polarization has resulted in a signal enhancement of the hydroxyl ^{17}O nuclei, as the integrated intensity of this site has increased by 33% relative to the spectrum in Fig. 4a (recorded in the same total experiment time). The signal enhancement observed in this system, compared with the large reductions in signal observed in the ^{23}Na example above, may be attributed to the lower abundance, lower gyromagnetic ratio, and large quadrupolar coupling constant of the ^{17}O nucleus.

The three-quantum cross-polarized ^{17}O MAS NMR spectrum of boehmite is shown in Fig. 4c. As with conventional cross-polarization, the experiment is preferentially selective for the broader ^{17}O resonance. Slightly more of the narrow peak is observed in this spectrum, although this has only 1% of its intensity in the conventional spectrum in Fig. 4a. Although, comparing Figs. 4b and 4c, three-quantum cross-polarization appears much less efficient than conventional cross-polarization, it should be remembered that most of this sensitivity difference arises from the inefficient conversion of three- to observable single-quantum coherences that is common to all three-quantum MAS NMR experiments. In fact, the spectrum in Fig. 4c contains more than 90% of the signal intensity of a conventional three-quantum filtered spectrum (not shown) recorded in the same total experiment time.

It is important to note that the interpretation of the editing observed in both single- and three-quantum cross-polarized spectra should be treated with great care. The rate at which the cross-polarized signal builds up during the spin-locking period or contact time is dependent upon several parameters, including a strong inverse dependence upon the distance between the two spin systems. Figure 5a shows that, at short contact times, a strong single-quantum cross-polarization signal is obtained from those boehmite ^{17}O nuclei closest to ^{1}H, as observed in Fig. 4b. The cross-polarized signal from the nonprotonated O site builds up at a slower rate but, as the contact time is increased, this ^{17}O signal eventually dominates the spectrum, the hydroxyl ^{17}O signal having decayed away. Figure 5b shows that a similar contact time dependence is observed for three-quantum cross-polarization. Figures 5a and 5b demonstrate, therefore, that a poor choice of contact time might lead to an incorrect assignment of the two O species. The rate at which the cross-polarized signal builds up also depends upon the ratio of ω_{1S} to ω_{Q}^{PAS} and, if cross-polarization is performed at differ-

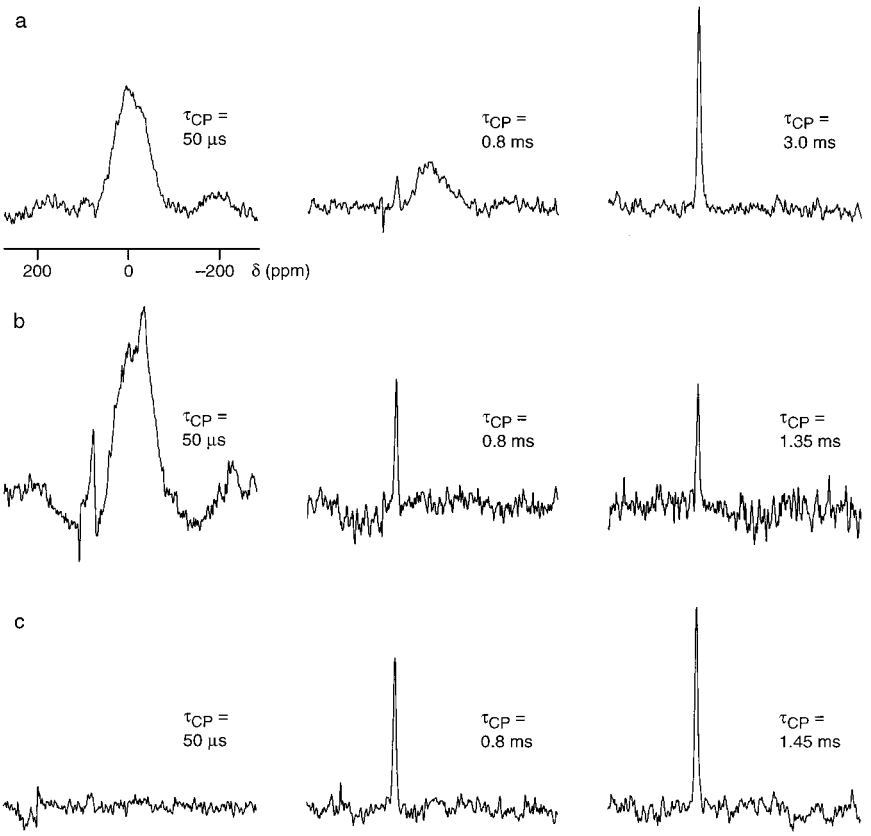

FIG. 5. Cross-polarized ^{17}O MAS NMR spectra of 35% isotopically enriched boehmite. (a) Single-quantum cross-polarized spectra with an ^{17}O radiofrequency field strength of $\omega_{1S}/2\pi = 25$ kHz, a ^{1}H field strength of $\omega_{1I}/2\pi = 77$ kHz, and contact times (τ_{CP}) of 50 μs, 800 μs, and 3 ms. (b) Three-quantum cross-polarized spectra with an ^{17}O radiofrequency field strength of $\omega_{1S}/2\pi = 80$ kHz, a ^{1}H radiofrequency field strength of $\omega_{1I}/2\pi = 50$ kHz, and contact times (τ_{CP}) of 50 μs, 800 μs, and 1.35 ms. (c) Single-quantum cross-polarized spectra with an ^{17}O radiofrequency field strength of $\omega_{1S}/2\pi = 70$ kHz, a ^{1}H radiofrequency field strength of $\omega_{1I}/2\pi = 77$ kHz, and contact times (τ_{CP}) of 50 μs, 800 μs, and 1.45 ms. In (a) and (c) 48 transients were averaged, while in (b) 840 transients were averaged. The recycle interval was 1 s in each case. In all spectra the displayed spectral width is 30 kHz and the MAS rate was 9 kHz.

ent matching conditions, the relative selectivity with which the two ^{17}O resonances are observed may be affected. For example, Fig. 5c shows that single-quantum cross-polarization performed at a higher ω_{1S} field strength than that used in Figs. 4b and 5a is entirely selective for the narrow (low P_Q) ^{17}O resonance, i.e., nonprotonated O site. Similar changes in preferential selectivity, which again might lead to an incorrect assignment, can also be observed in three-quantum cross-polarization.

The two-dimensional three-quantum ^{17}O MAS NMR spectrum of boehmite, recorded using a *z*-filter, is shown in Fig. 6a. The spectrum is dominated by the narrow resonance from the Al–O–Al linkage, with the signal from the broader hydroxyl resonance barely observable even at significantly lower contours than those used in Fig. 6a. The two-dimensional ^{17}O MQCP-MQMAS spectrum of boehmite, recorded with the three-quantum cross-polarized pulse sequence in Fig. 1a, is shown in Fig. 6b. In this spectrum the broader ^{17}O resonance is clearly visible since the three-quantum cross-polarization appears to be preferentially selective for this site. This can also be judged from the relative integrated intensities of the two ridges, which in this spectrum are 1:4.4, compared with 1:0.43 in the spectrum in Fig. 6a. The two-dimensional spectrum in Fig. 6b is proof that the broader ^{17}O resonance observed in the conventional MAS NMR spectrum of boehmite is indeed a single second-order broadened ^{17}O lineshape, corresponding to a large P_Q value, and not a combination of more than one overlapping lineshape. The values of the isotropic chemical shift, δ_{CS}, and quadrupolar product, P_Q, extracted from the F_1 and F_2 positions of the ridge lineshapes (35 and 74 ppm and 5.5 and 1.1 MHz for the broad and narrow resonances, respectively) agree with those found in the literature (*8*).

The conventional ^{27}Al ($S = \frac{5}{2}$) MAS NMR spectrum of AlMePO-β, a novel microporous material (*45*, *46*), is shown in Fig. 7. In recent years, there has been much interest in microporous materials owing to their wide utility as ion exchange materials, catalysts, and adsorbents. The recently characterized aluminum methylphosphonate AlMePO-β has both six- and four-coordinate Al sites, as can be seen in Fig. 7 where there are characteristic ^{27}Al peaks near -18 and 40 ppm, respectively. Although a single octahedral resonance is predicted from the structure of AlMePO-β, three distinct tetrahedral

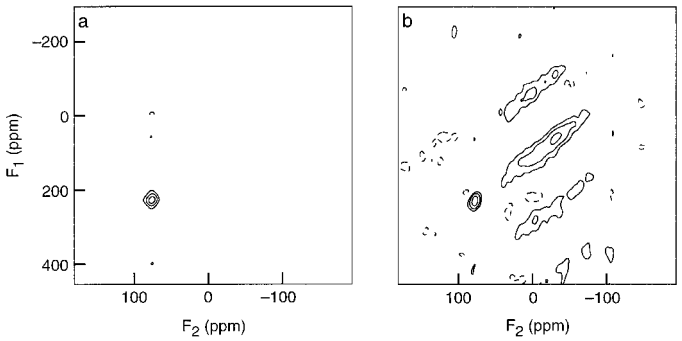

FIG. 6. Two-dimensional (a) three-quantum ^{17}O MAS and (b) three-quantum cross-polarized ^{17}O MAS NMR spectra of 35% isotopically enriched boehmite, recorded with (a) a three-quantum z-filtered experiment and (b) the pulse sequence displayed in Fig. 1a. In (a) 480 transients were averaged for each of 192 t_1 increments of 6.66 μs with a recycle interval of 1 s and in (b) 3600 transients were averaged for each of 72 t_1 increments of 6.66 μs with a recycle interval of 1 s. In both cases displayed F_1 and F_2 spectral widths are 40 and 20 kHz, respectively, and the MAS rate was 9 kHz. Contour levels are shown at 16, 32, and 64% of the maximum value. In (b) cross-polarization was performed with a ^{17}O radiofrequency field strength of $\omega_{1S}/2\pi = 80$ kHz, a ^{1}H field strength of $\omega_{1I}/2\pi = 50$ kHz, and a contact time of 100 μs.

resonances are expected. A large difference in chemical shift ensures good separation of the two different Al coordinations, but the presence of second-order quadrupolar broadening prevents the resolution of the three crystallographically distinct tetrahedral sites.

It has been shown previously that two-dimensional five-quantum ^{27}Al MAS NMR experiments are better at resolving the three distinct tetrahedral resonances in AlMePO-β than the corresponding three-quantum experiments as they yield a greater frequency separation (i.e., a factor of approximately 4.2 in the isotropic projection for spin $S = \frac{5}{2}$) (*41*, *47*). The tetrahedral region of the two-dimensional five-quantum ^{27}Al MAS NMR spectrum of AlMePO-β, recorded using the phase-modulated split-t_1 sequence of Ref. (*41*) is shown in Fig. 8a. Three ridge lineshapes parallel to the F_2 axis are clearly distinguishable, and analysis of their F_1 and F_2 positions yields P_Q values of 2.4, 1.9, and 1.8 MHz in order of decreasing ppm values (designated sites 1, 2, and 3, respectively). The isotropic projection onto the F_1 axis reveals three distinct resonances,

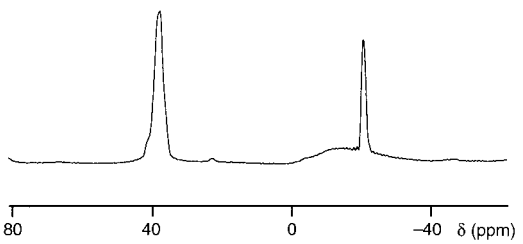

FIG. 7. Conventional ^{27}Al (104.3 MHz) MAS NMR spectrum of AlMePO-β. The spectrum is the result of averaging 48 transients with a 2-s recycle interval. The displayed spectral width is 15 kHz and the MAS rate was 4.5 kHz. The ppm scale is referenced to 1 M $Al(NO_3)_3$ (aq).

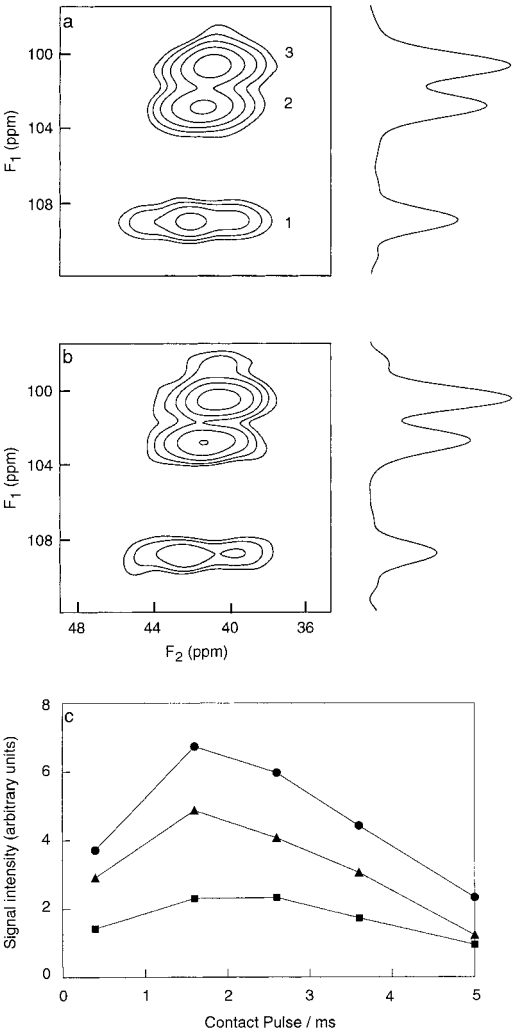

FIG. 8. Two-dimensional (a) five-quantum ^{27}Al MAS and (b) five-quantum cross-polarized ^{27}Al MAS NMR spectra of AlMePO-β, recorded with (a) a phase-modulated five-quantum split-t_1 experiment and (b) the pulse sequence displayed in Fig. 1b denoted by the dotted coherence pathway. In both (a) and (b) 320 transients were averaged for each of 64 t_1 increments of 100 μs with a recycle interval of 2 s. In both cases displayed F_1 and F_2 spectral widths are 1.5 kHz and the MAS rate was 4.5 kHz. Contour levels are shown at 4, 8, 16, 32, and 64% of the maximum value. In (b) cross-polarization was performed with a ^{27}Al radiofrequency field strength of $\omega_{1S}/2\pi = 100$ kHz, a ^{1}H field strength of $\omega_{1I}/2\pi = 50$ kHz, and a contact time of 2 ms. (c) Plot of ^{27}Al NMR signal intensity (extracted from a series of two-dimensional five-quantum cross-polarized MAS spectra) for each distinct site in AlMePO-β as a function of the contact time. Cross-polarization was performed with radiofrequency field strengths as in (b). Filled squares, triangles, and circles signify sites 1, 2, and 3, respectively.

with the one corresponding to the largest P_Q value (site 1) having a slightly lower intensity owing to the nonuniform excitation and conversion of the five-quantum coherences.

Figure 8b shows the corresponding tetrahedral region of a two-dimensional five-quantum cross-polarized ^{27}Al MAS NMR spectrum, recorded with the pulse sequence shown in Fig. 1b (dotted coherence transfer pathway) with $k = 12/37$

and $k' = 25/37$. All three tetrahedral-region ^{27}Al resonances are observed in this spectrum, showing the proximity of all three to ^{1}H nuclei, a conclusion unobtainable from the conventional CPMAS NMR spectrum alone. The isotropic projection in Fig. 8b shows that the relative intensities of the three ^{27}Al peaks have changed slightly from those observed in Fig. 8a. As discussed above, however, these relative intensities may depend upon a number of factors, including (i) the ratio of ω_{1S} to ω_Q^{PAS} (although, in this case, the ω_Q^{PAS} values for the three peaks appear to be similar), (ii) the strong inverse IS distance dependence of cross-polarization and, strongly related to these first two factors, (iii) the choice of contact time.

By performing the two-dimensional MQCP-MQMAS experiment for a range of values of the contact time, it is possible to monitor the buildup and decay of each tetrahedral-region ^{27}Al resonance individually, allowing the possibility of extracting distance information (*48*). Figure 8c shows the integrated intensity of each ^{27}Al resonance (arbitrary scale) against contact time for each of the three tetrahedrally coordinated sites in AlMePO-β. Although many more values of the contact time would be needed in order to extract any quantitative information, the five-quantum cross-polarization profiles of the three sites do indeed show small differences. Site 1 (denoted by squares) shows a maximum ^{27}Al signal intensity at significantly longer durations of the contact time than sites 2 (triangles) and 3 (circles), while the decay of this site 1 signal is also less rapid than in the other two sites. Site 2 shows the most rapid signal decay, with its intensity at 5-ms contact time being almost equal to that of site 1. Although Fig. 8c shows that the ^{27}Al signal intensity of site 1 is maximized relative to the other two sites at longer contact times, perhaps indicating a greater distance from ^{1}H, this intensity is always lower than that observed for sites 2 and 3. This is probably due, in part, to the lower efficiency of five-quantum conversion for this site, a feature also observed in the conventional five-quantum ^{27}Al MAS NMR spectrum in Fig. 8a.

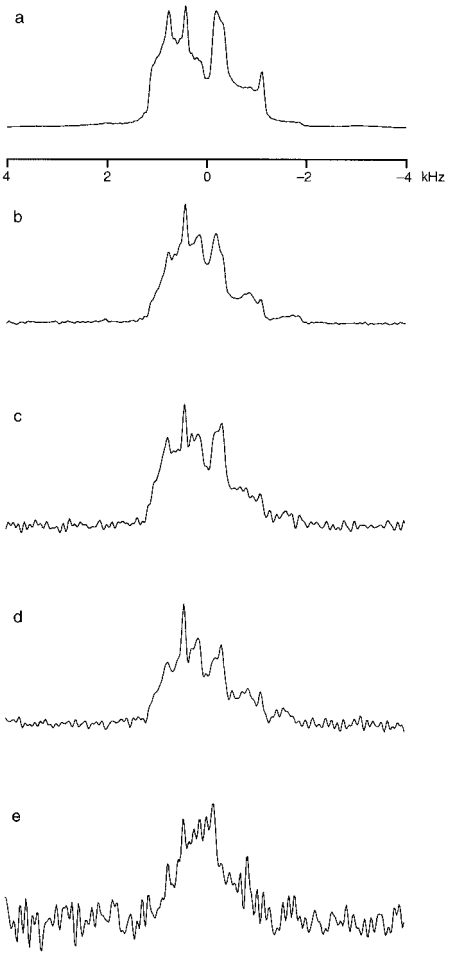

FIG. 9. (a) Conventional, (b) single-quantum cross-polarized, (c) three-quantum cross-polarized, (d) five-quantum cross-polarized, and (e) seven-quantum cross-polarized ^{45}Sc (97.2 MHz) MAS NMR spectra of scandium sulfate pentahydrate ($Sc_2(SO_4)_3.5H_2O$). In all experiments 480 transients were averaged with a 5-s recycle interval. Cross-polarization was performed with ^{45}Sc radiofrequency field strengths of $\omega_{1S}/2\pi = 100$ kHz, ^{1}H field strengths of (b) $\omega_{1I}/2\pi = 77$ kHz, (c) and (d) $\omega_{1I}/2\pi = 50$ kHz, and (e) $\omega_{1I}/2\pi = 65$ kHz, and a contact time of 1 ms in all experiments. In all spectra the displayed spectral width is 8 kHz and the MAS rate was 6.5 kHz.

3.3. Multiple-Quantum Cross-Polarized MQMAS and Higher Spin Quantum Numbers

In nuclei with higher spin quantum numbers the possibility exists of direct cross-polarization to a range of multiple-quantum coherences, e.g., up to $n = 7$ for nuclei with $S = \frac{7}{2}$. In principle, any multiple-quantum coherence can be cross-polarized but the matching parameters (i.e., the two radiofrequency field strengths, ω_{1I} and ω_{1S}, and the contact time) for optimum cross-polarization will differ from one coherence order to another and are best determined experimentally in each case, perhaps with the aid of a multiple-quantum nutation experiment.

Figure 9a shows the conventional ^{45}Sc ($S = \frac{7}{2}$) MAS NMR spectrum of scandium sulfate pentahydrate ($Sc_2(SO_4)_3.5H_2O$). This spectrum consists of a superposition of three second-order broadened lineshapes, corresponding to three distinct Sc sites, all of which possess relatively low P_Q values (*49*). Figures 9b, 9c, 9d, and 9e show the ^{45}Sc MAS NMR spectra of scandium sulfate resulting from cross-polarization to single-, three-, five-, and seven-quantum coherences, respectively. Each exhibits lineshape distortion characteristic of differences in cross-polarization efficiency between the crystallites within a single ^{45}Sc lineshape and of differences in efficiency between the three ^{45}Sc lineshapes. These results show that it is feasible to cross-polarize with relative ease from ^{1}H to all of the higher order ^{45}Sc multiple-quantum coherences, although this is possibly a reflection of the relatively low P_Q values found in this sample. On first inspection, the efficiency of cross-polarization appears to decrease with increasing coherence order, i.e., the spectra in Figs. 9b–9e contain only 5.1, 1.2, 0.9, and 0.3% of

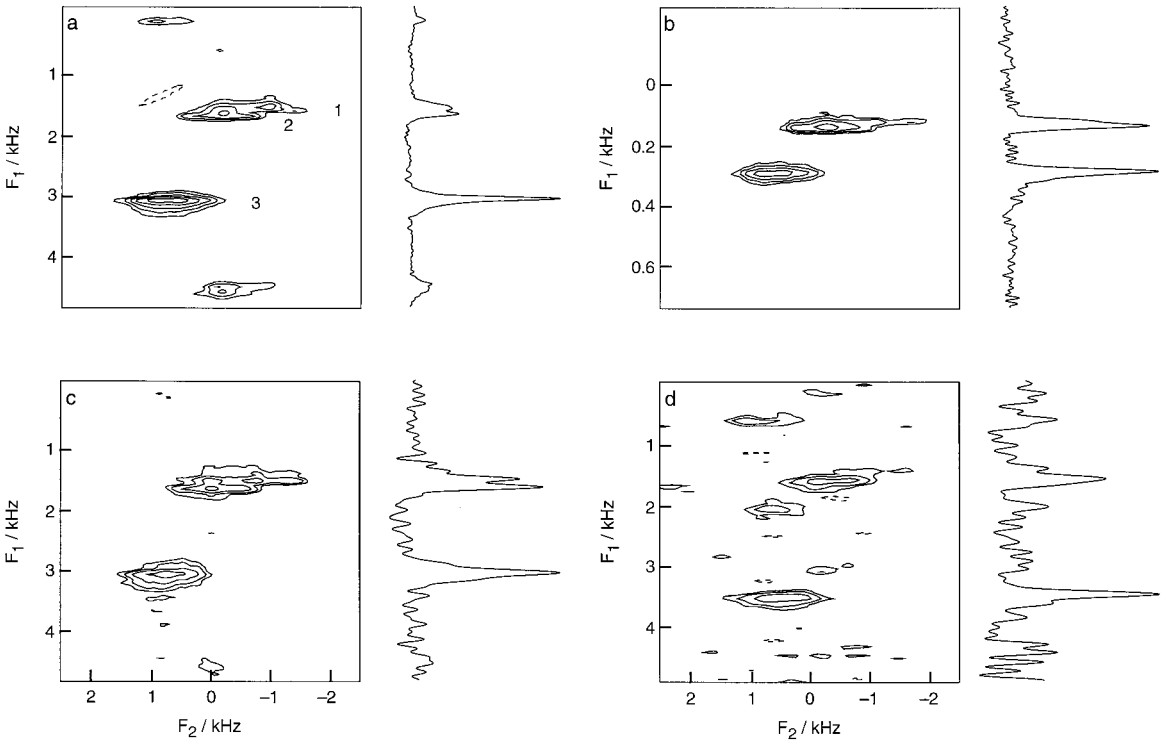

FIG. 10. Two-dimensional (a) five-quantum ^{45}Sc MAS, (b) three-quantum cross-polarized ^{45}Sc MAS, (c) five-quantum cross-polarized ^{45}Sc MAS, and (d) seven-quantum cross-polarized ^{45}Sc MAS NMR spectra of scandium sulfate. The spectra were recorded with (a) a phase-modulated split-t_1 five-quantum experiment, (b) and (c) the pulse sequence displayed in Fig. 1c with solid and dotted coherence transfer pathways, respectively, and (d) the pulse sequence displayed in Fig. 1b with the dashed coherence transfer pathway. In (a) 160 transients were averaged for each of 256 t_1 increments of 66.6 μs, with a recycle interval of 3 s; in (b) 192 transients were averaged for each of 256 t_1 increments of 200 μs, with a recycle interval of 5 s; in (c) 320 transients were averaged for each of 256 t_1 increments of 66.6 μs, with a recycle interval of 3 s; and in (d) 360 transients were averaged for each of 192 t_1 increments of 40 μs, with a recycle interval of 5 s. In (a), (c), and (d) displayed F_1 and F_2 spectral widths are 5 kHz, while in (b) displayed F_1 and F_2 spectral widths are 1.25 and 5 kHz, respectively. In all experiments the MAS rate was 6.5 kHz. Contour levels are shown at (a) 4, 8, 16, 32, and 64%, (b) and (c) 8, 16, 32, and 64%, and (d) 16, 32, and 64% of the maximum value. Cross-polarization was performed with ^{45}Sc radiofrequency field strengths of $\omega_{1S}/2\pi = 100$ kHz, ^{1}H field strengths of (b) $\omega_{1I}/2\pi = 66$ kHz, (c) and (d) $\omega_{1I}/2\pi = 50$ kHz, and contact times of (b) and (c) 1 ms and (d) 400 μs.

the intensity of the conventional spectrum in Fig. 9a. It should be noted, however, that this corresponds to 5.1, 9.2, 19.7, and 20.1% of the intensity obtained from conventional (i.e., "pulse-acquire" or "single-quantum") and three-, five-, and seven-quantum filtered experiments, respectively.

Although cross-polarized spectra can be obtained in this system, the exact nature or number of the distinct ^{45}Sc nuclei involved cannot be determined using the results in Fig. 9. Two-dimensional methods must be employed so that a more detailed description of the results of cross-polarization may be obtained. Cross-polarization to higher order multiple-quantum coherences is of interest since the use of such coherences in MQMAS experiments yields greater frequency dispersion, and hence higher resolution, in the isotropic projections of MQ-MAS spectra (*49*).

The two-dimensional five-quantum ^{45}Sc MAS NMR spectrum shown in Fig. 10a, recorded using a five-quantum split-t_1 experiment (*49*), reveals two closely spaced ^{45}Sc ridge lineshapes, with a third lineshape at higher frequency with approximately twice the intensity of either of the other two. The values of the quadrupolar parameters, e^2qQ/h and η, extracted from each lineshape, are 5.2, 4.3, and 4.5 MHz and 0.1, 0.8, and 0.5 for sites 1, 2, and 3 (in order of increasing F_1 values), respectively (*49*). Two-dimensional three-, five-, and seven-quantum cross-polarized ^{45}Sc MAS NMR spectra of scandium sulphate are shown in Figs. 10b, 10c, and 10d, respectively. The three- and five-quantum MAS spectra in Figs. 10b and 10c were recorded with the cross-polarized split-t_1 experiment in Fig. 1c with $k = 45/146$ and $k' = 101/146$ for three-quantum and $k = 9/20$ and $k' = 11/20$ for five-quantum. The seven-quantum MAS spectrum in Fig. 10d was recorded with the cross-polarized split-t_1 experiment in Fig. 1b with $k = 45/206$ and $k' = 161/206$.

The three-quantum cross-polarized MAS spectrum in Fig. 10b does not quite allow complete resolution of the two closely spaced resonances, but the presence of three sites can be deduced with care. This spectrum also shows that cross-polarization to all three sites is observed, and, although the signal intensity from site 3 is still greater than that from sites 1 and 2, it no longer possesses

twice the intensity. This might reflect the fact that site 3 could be further from ^{1}H nuclei and, consequently, cross-polarization might select against this site. However, the fact that the site 3 signal is further off resonance than the site 1 and 2 signals should also be considered a possible explanation, although we have found that cross-polarization with the site 3 signal on resonance does not yield a significant increase in intensity. The five-quantum cross-polarized spectrum (Fig. 10c) does allow the site 1 and 2 lineshapes to be resolved, the increase in F_1 frequency dispersion being immediately apparent. Again, it appears that cross-polarization is relatively less efficient for site 3. The seven-quantum cross-polarized spectrum in Fig. 10d has a low signal-to-noise ratio as a consequence of the inefficiency of both seven-quantum cross-polarization and the conversion to single-quantum coherences. As a result, only sites 2 and 3 are present in the spectrum at a significant level of intensity with site 1 appearing at low contour levels only. However, seven-quantum cross-polarization appears relatively more efficient at site 3 than in three- and five-quantum cross-polarization, while for site 1 the opposite is true, and again this indicates that off-resonance effects are relatively unimportant.

4. CONCLUSIONS

We have shown that a combination of direct multiple-quantum cross-polarization and the high-resolution MQMAS NMR experiment provides a potentially useful tool for the study of structural relationships in systems containing quadrupolar nuclei. The demonstration of the technique in systems of differing spin quantum number, gyromagnetic ratio, and relative nuclide abundance and the use of cross-polarization to higher order multiple-quantum coherences show that the method is applicable across a wide range of samples and chemical problems. The spectral editing capability of cross-polarization, as demonstrated on boehmite using ^{17}O MAS NMR, allows important spectral and possibly structural information to be obtained. The combined MQCP-MQMAS technique also enables the cross-polarization dynamics of individual crystallographically distinct sites to be extracted, information that is unavailable from conventional MAS NMR. In order to extract detailed structural parameters from these measurements a more detailed theoretical understanding of multiple-quantum cross-polarization under MAS conditions is required and is, therefore, an important future aim.

ACKNOWLEDGMENTS

We are grateful to EPSRC for generous support (Grant GR/M12209 and the award of a studentship to S.E.A.). We also thank Dr. A. J. Berry (Australian National University, Canberra) for synthesizing the ^{17}O-enriched boehmite sample, Dr. V. J. Carter (University of St. Andrews, Scotland) for providing the sample of AlMePO-β, Dr. P. Hodgkinson for writing the two-dimensional Fourier transform program, and Dr. K. J. Pike for help with optimising the seven-quantum phase cycle.

REFERENCES

1. S. R. Hartmann and E. L. Hahn, *Phys. Rev.* **128,** 2042 (1962).
2. A. Pines, M. G. Gibby, and J. S. Waugh, *J. Chem. Phys.* **56,** 1776 (1972).
3. R. K. Harris and G. J. Nesbitt, *J. Magn. Reson.* **78,** 245 (1988).
4. S. Hayashi, *Solid State Nucl. Magn. Reson.* **3,** 93 (1994).
5. D. E. Woessner, *Z. Phys. Chem. Neue Fol.* **152,** 51 (1987).
6. J. C. Edwards and P. D. Ellis, *Magn. Reson. Chem.* **28,** S59 (1990).
7. T. H. Walter, G. L. Turner, and E. Oldfield, *J. Magn. Reson.* **76,** 106 (1988).
8. T. H. Walter and E. Oldfield, *J. Phys. Chem.* **93,** 6744 (1989).
9. M. G. Mortuza, R. Dupree, and S. C. Kohn, *Appl. Magn. Reson.* **4,** 89 (1993).
10. H. D. Morris, S. Bank, and P. D. Ellis, *J. Phys. Chem.* **94,** 3121 (1990).
11. P. J. Barrie, *Chem. Phys. Lett.* **208,** 486 (1993).
12. R. G. Bryant, S. Ganapathy, and S. D. Kennedy, *J. Magn. Reson.* **72,** 376 (1987).
13. S. Ganapathy, S. Schramm, and E. Oldfield, *J. Phys. Chem.* **77,** 4360 (1982).
14. L. Frydman and J. S. Harwood, *J. Am. Chem. Soc.* **117,** 5367 (1995).
15. A. Medek, J. S. Harwood, and L. Frydman, *J. Am. Chem. Soc.* **117,** 12779 (1995).
16. J. H. Baltisberger, Z. Xu, J. F. Stebbins, S. H. Wang, and A. Pines, *J. Am. Chem. Soc.* **118,** 7209 (1996).
17. P. Sarv, C. Fernandez, J. P. Amoureux, and K. Keskinen, *J. Phys. Chem.* **100,** 19223 (1996).
18. S. J. Hwang, C. Fernandez, J. P. Amoureux, J. Cho, S. W. Martin, and M. Pruski, *Solid State Nucl. Magn. Reson.* **8,** 109 (1997).
19. M. Pruski, D. P. Lang, C. Fernandez, and J. P. Amoureux, *Solid State Nucl. Magn. Reson.* **7,** 327 (1997).
20. C. Fernandez, L. Delevoye, J. P. Amoureux, D. P. Lang, and M. Pruski, *J. Am. Chem. Soc.* **119,** 6858 (1997).
21. J. P. Amoureux, C. Fernandez, and S. Steuernagel, *J. Magn. Reson. A* **123,** 116 (1996).
22. S. E. Ashbrook, S. P. Brown, and S. Wimperis, *Chem. Phys. Lett.* **288,** 509 (1998).
23. K. H. Lim and C. P. Grey, *Chem. Phys. Lett.* **312,** 45 (1999).
24. K. H. Lim and C. P. Grey, *J. Chem. Phys.* **112,** 7490 (2000).
25. D. Rovnyak, M. Baldus, and R. G. Griffin, *J. Magn. Reson.* **142,** 145 (2000).
26. E. O. Stejskal, J. Schaefer, and J. S. Waugh, *J. Magn. Reson.* **28,** 105 (1977).
27. S. Vega, T. W. Shattuck, and A. Pines, *Phys. Rev. A* **22,** 638 (1980).
28. L. Müller, R. Eckman, and A. Pines, *Chem. Phys. Lett.* **76,** 149 (1980).
29. P. Brunner, M. Reinhold, and R. R. Ernst, *J. Chem. Phys.* **73,** 1086 (1980).
30. M. Reinhold, P. Brunner, and R. R. Ernst, *J. Chem. Phys.* **74,** 184 (1981).
31. S. Vega, *Phys. Rev. A* **23,** 3152 (1981).
32. S. E. Ashbrook and S. Wimperis, *Mol. Phys.* **98,** 1 (2000).
33. A. J. Vega, *Solid State Nucl. Magn. Reson.* **1,** 17 (1992).

34. N. C. Nielsen, H. Bildsøe, and H. J. Jakobsen, *J. Magn. Reson.* **97,** 149 (1992).

35. S. Ding and C. A. McDowell, *J. Magn. Reson. A* **114,** 36 (1995).

36. A. J. Vega, *J. Magn. Reson.* **96,** 50 (1992).

37. G. Bodenhausen, H. Kogler, and R. R. Ernst, *J. Magn. Reson.* **58,** 370 (1984).

38. S. P. Brown, S. J. Heyes, and S. Wimperis, *J. Magn. Reson. A* **119,** 280 (1996).

39. S. P. Brown and S. Wimperis, *J. Magn. Reson.* **124,** 279 (1997).

40. S. P. Brown and S. Wimperis, *J. Magn. Reson.* **128,** 42 (1997).

41. S. P. Brown, S. E. Ashbrook, and S. Wimperis, *J. Phys. Chem. B* **103,** 812 (1999).

42. T. Vosegaard, P. Florian, P. J. Grandinetti, and D. Massiot, *J. Magn. Reson.* **143,** 217 (2000).

43. K. T. Mueller, J. H. Baltisberger, E. W. Wooten, and A. Pines, *J. Phys. Chem.* **96,** 7001 (1992).

44. G. Wu, D. Rovnyak, and R. G. Griffin, *J. Am. Chem. Soc*. **118,** 9326 (1996).

45. K. Maeda, Y. Kiyozumi, and F. Mizukami, *Agnew. Chem. Int. Ed. Engl.* **33,** 2335 (1994).

46. V. J. Carter, P. A. Wright, J. D. Gale, R. E. Morris, E. Sastre, and J. Perez-Pariente, *J. Mater. Chem.* **7,** 2287 (1997).

47. J. Rocha, Z. Lin, C. Fernandez, and J. P. Amoureux, *Chem. Commun.* 2513 (1996).

48. M. Mehring, "Principles of High Resolution NMR in Solids," Springer-Verlag, Berlin, 1983.

49. K. J. Pike, R. P. Malde, S. E. Ashbrook, J. McManus, and S. Wimperis, *Solid State Nucl. Magn. Reson.* **16,** 203 (2000).